Restraining growth of Zn dendrites by poly dimethyl diallyl ammonium cations in aqueous electrolytes

Xiang-Xin Zhang, Yuan-Qiang Chen, Chang-Xin Lin, Yuan-Sheng Lin, Guo-Lin Hu, Yong-Chuan Liu, Xi-Lai Xue, Su-Jing Chen, Zhan-Lin Yang, Bai-Sheng Sa*, Yi-Ning Zhang*

Abstract Metallic zinc is an excellent anode material for Zn-ion batteries, but the growth of Zn dendrite severely hinders its practical application. Herein, an efficient and economical cationic additive, poly dimethyl diallyl ammonium (PDDA) was reported, used in aqueous Zn-ion batteries electrolyte for stabilizing Zn anode. The growth of zinc dendrites can be significantly restrained by benefiting from the pronounced electrostatic shielding effect from PDDA on the Zn metal surface. Moreover, the PDDA is preferentially absorbed on Zn (002) plane, thus preventing unwanted side reactions on Zn anode. Owing to the introduction of a certain amount of PDDA additive into the common $ZnSO_4$-based electrolyte, the cycle life of assembled Zn||Zn cells (1 $mA{\cdot}cm^{-2}$ and 1 $mAh{\cdot}cm^{-2}$) is prolonged to more than 1100 h. In response to the perforation issue of Zn electrodes caused by PDDA additives, the problem can be solved by combining foamy copper with zinc foil. For real application, Zn-ion hybrid supercapacitors and MnO_2||Zn cells were assembled, which exhibited excellent cycling stability with PDDA additives. This work provides a new solution and perspective to cope with the dendrite growth problem of Zn anode.

Keywords PDDA; Electrostatic shielding effect; Zn anode; Zn dendrites

1 Introduction

The aqueous rechargeable Zn-ion batteries (ZIBs) are extremely attractive in the field of energy storage systems, due to the combination of high theoretical capacity of Zn metal anode (820 $mAh{\cdot}g^{-1}$), low redox potential (− 0.76 V vs. standard hydrogen electrode), enhanced safety and low cost [1–3]. However, the Zn metal anode faces great challenges of dendritic Zn growth and interfacial side reactions, largely limiting the practical applications of ZIBs [1, 4]. The main reason for the growth of Zn dendrites is the presence of the uneven charge distribution at the electrolyte/electrode interface, which causes irregular zinc deposition [5]. Moreover, the freshly deposited Zn exists the tip effect and is more susceptible to generate side reactions (e.g., production of $Zn_4(OH)_6SO_4{\cdot}xH_2O$ or H_2 releasing), which might short circuit the ZIBs and lead to poor cycle stability [6]. Therefore, regulating the Zn^{2+} disposition and restraining the dendrite growth of Zn metal anodes are the key to breaking the above-mentioned bottlenecks, to meet people's demand for the application of clean energy [7–10].

Building a viable protective layer or artificial solid electrolyte interphase (SEI) can be considered as a direct

X.-X. Zhang, Y.-Q. Chen, C.-X. Lin, Y.-S. Lin, G.-L. Hu, Y.-C. Liu, S.-J. Chen, Y.-N. Zhang*
Key Laboratory of Optoelectronic Materials Chemistry and Physics, Fujian Institute of Research on the Structure of Matter, Chinese Academy of Sciences, Fuzhou 350002, China
e-mail: ynzhang@fjirsm.ac.cn

X.-L. Xue
Helmholtz Institute Ulm (HIU), 89081 Ulm, Germany

X.-L. Xue
Karlsruhe Institute of Technology (KIT), 76021 Karlsruhe, Germany

Z.-L. Yang, B.-S. Sa*
College of Materials Science and Engineering, Fuzhou University, Fuzhou 350108, China
e-mail: bssa@fzu.edu.cn

solution to block the dendrite growth and reduce side reactions [11, 12]. Inorganic metal compounds (e.g., TiO_2, Al_2O_3, ZnF_2 and ZnS) usually serve as protective layers to mitigate dendrite growth [13–16]. Nevertheless, it should be noted that some protective layer synthesis can be intricate and constrained by the electrode shape. For example, a Zn anode with nitrogen-doping interface is synthesized by plasma surface treatment [17]. Although nitrogen-doping technology could improve Zn anode stability and suppress dendrite growth to some extent, the high-frequency plasma generator is expensive and requires more time to synthesize. Compared with the above-mentioned methods, the electrolyte engineering is a simple way to improve the growth of Zn dendrites [18, 19]. The most common method involves the incorporation of various nonionic compounds as electrolyte additives, such as methanol, dimethyl sulfoxide, dimethyl carbonate, and ethylene glycol [20–23]. By lone pair electron interaction with Zn^{2+}, the nonionic molecule substitutes H_2O in the $[Zn(H_2O)_6]^{2+}$ solvation structure in aqueous $ZnSO_4$-based electrolyte, minimizing water activity and directing Zn^{2+} deposition [7]. In addition, ionic compounds are often used as additives. Inspired by cation additives in lithium-ion batteries, it was found that some cation additives could also provide an electrostatic shielding effect on the Zn surface to hinder dendrite growth [24]. For example, when the Na_2SO_4 is added into the electrolyte, the Zn^{2+} and Na^+ are adsorbed simultaneously on the Zn metal surface during Zn anode reduction process, due to the lower reduction potential of Na^+ than that of Zn^{2+} [25]. During the Zn^{2+}-deposition process, there is a preferential reduction of Zn^{2+} over Na^+. Subsequently, the Na^+ continues to adhere to Zn metal surface, aggregating around the protuberant tips, and forming a local electrostatic shielding layer to drive Zn^{2+} to deposit in adjacent regions of the anode, leading to the formation of a smoothly deposited layer that significantly restrains dendrite growth. It is worth mentioning that this phenomenon extends beyond common inorganic cation ion (e.g., Li^+, K^+ and NH_4^+) [26–28]. Organic cation includes cholinium cations, triethylmethyl ammonium and tetrabutylammonium [5, 29, 30]. Diethylamine hydrochloride homologues was studied and found that Zn dendrites was significantly inhibited with number of methyl increasing [4]. To improve the performance, a large quantity of organic additives were introduced (over 1 $mol{\cdot}L^{-1}$). However, this approach led to an undesirable increase in polarization for ZIBs, which had a negative impact on cell performance. In this regard, an efficient additive to suppress dendrite formation without causing additional negative effects should be discovered [4].

Polymer electrolyte additives are a kind of effective additive. Li et al. [31] used the PEG200 to regulate dendrite growth to improve the long-term cycling stability of aqueous rechargeable Zn||Zn batteries. Huang et al. [32] took advantage of Zn^{2+} adsorption on the acyl group of polyacrylamide (PAM), which was subsequently carried throughout the polymer chain, resulting in a homogeneous Zn distribution on the electrode surface. Polyvinylpyrrolidone (PVP) acted as a highly efficiency electrolyte additive, exerting a significant influence on Zn dendrite inhibition during electroplating process. Relying on electrostatic power and spatial resistance of PVP, a small amount of PVP brought about excellent results for ZIBs [33].

In this study, a poly dimethyl diallyl ammonium (PDDA) cation polymer was introduced as an additive to $ZnSO_4$ electrolyte. PDDA, a typical cation ion polymer, offers a plethora of advantages including low toxicity, chemically stable, and easy to synthetize [34, 35]. PDDA possesses strong electrostatic shielding effect for Zn metal anode, accompanied by favorable absorption property on Zn surface. A small amount of PDDA fulfills the requirements of regulating Zn^{2+} disposition and restraining dendrite growth. Moreover, PDDA is preferentially absorbed onto Zn (002) plane to protect Zn electrode from side reactions. The cycle life of assembled Zn||Zn cells (1 $mA{\cdot}cm^{-2}$ and 1 $mAh{\cdot}cm^{-2}$) is prolonged from less than 150 h to more than 1100 h. To tackle the issues of Zn electrode perforation caused by PDDA additive, a solution involves the combination of more foamy copper with Zn foil. Furthermore, the Zn-ion hybrid supercapacitors (ZHCs) and MnO_2||Zn batteries display long cycle life with PDDA additive.

2 Results and discussion

2.1 Function of PDDA

In order to elucidate the solventized structure of Zn^{2+} formed by PDDA with ions (Zn^{2+} and SO_4^{2-}) in the electrolyte, the physicochemical properties of several electrolytes and compounds were investigated in this work. Figure 1a shows the possible structure of PDDA with $ZnSO_4$. Since the quaternary ammonium functional group of positive ions can effectively attract negative ions, the sulfate ion (SO_4^{2-}) is close to the quaternary ammonium part of PDDA additive. To substantiate this phenomenon, Raman and nuclear magnetic resonance (NMR) were used to directly characterize the solvation structures of electrolytes. Raman spectra (Fig. 1b) demonstrate that the SO_4^{2-} signal experiences a redshift, which indicates that the environment around SO_4^{2-} has been changed by PDDA [5]. In turn, the environment around PDDA has also been changed by SO_4^{2-}. According to the molecule structure of PDDA, it is notable that two methyl groups are directly

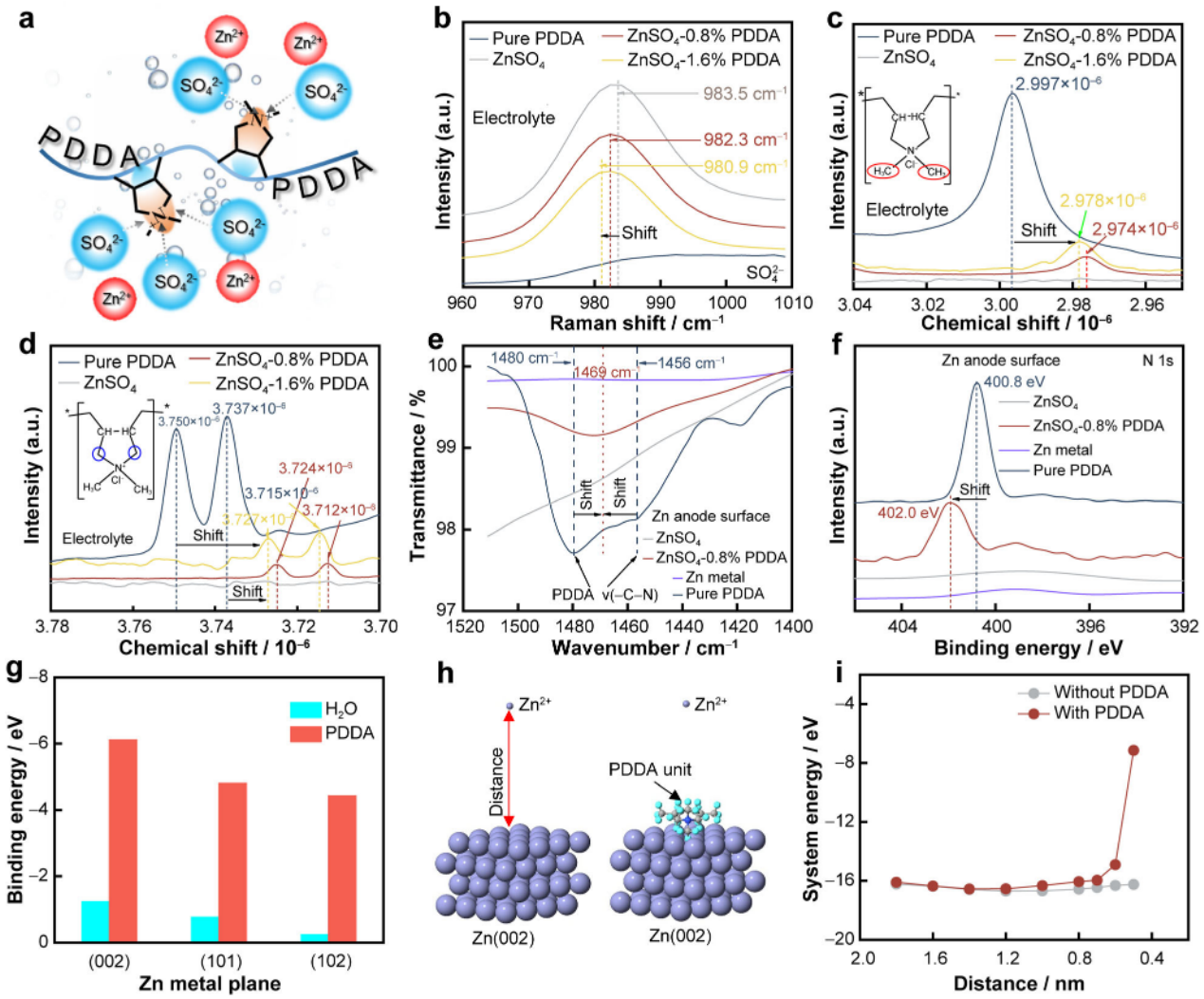

Fig. 1 Characterizations of electrolyte structure: **a** schematic diagram of PDDA cations in $ZnSO_4$ electrolytes; **b** Raman spectra of electrolytes between 960 and 1010 cm ^{1} (SO_4^{2} signal); **c, d** ^{1}H of methyl and methylene groups NMR spectra of different electrolytes; **e** FTIR spectra; **f** XPS spectra; **g** binding energy of PDDA and H_2O on Zn plane; **h** model of DFT calculations, showing a Zn^{2+} closing to Zn (002) plane with or without PDDA unit; and **i** system energy of Zn^{2+} close to Zn (002) plane

bonded to nitrogen atom (positive charge). The proximity of SO_4^{2-} to nitrogen atom can affect the surrounding environment of these two methyl groups. PDDA methyl ^{1}H of methyl groups NMR spectra and the full ^{1}H NMR spectra are shown in Figs. 1c, S1a, respectively. For pure PDDA, the methyl peak is at 2.996×10^{-6}. With $ZnSO_4$ adding, the characteristic peak undergoes an up-field shift from 2.996×10^{-6} to 2.975×10^{-6}. The reason for the above phenomenon is that the rich-electron SO_4^{2-} partially replaces Cl^- and is close to nitrogen atom of PDDA, leading to the enhancement of charge shielding and changing position of methyl NMR peak [36]. Similarly, the methylene peak shifts to up-field, as shown in Fig. 1d. These results prove that SO_4^{2-} tends to nitrogen atom of PDDA. Moreover, Zn^{2+} tends to associate with SO_4^{2-} and neighboring PDDA in the electrolytes. The surrounding environment of zinc ions and the overall electrolyte structure has been modified by PDDA.

In addition to the solvation structure of the electrolyte, the interaction between PDDA and Zn metal surface was also studied. Fourier-transform infrared (FTIR) and X-ray photoelectron spectroscopy (XPS) were employed to investigate the interaction. Zn foils were soaked in $ZnSO_4$ and $ZnSO_4$-0.8% PDDA electrolytes for 24 h and ultrasonic washed by deionized water several times to remove residual electrolyte, respectively. FTIR peaks at 3150–2778 and 1502–1391 cm^{-1} could be ascribed to the bending vibration of $–CH_2–$ and –C–N of PDDA (Fig. S1b) [37]. The peaks at 1225–1003 cm^{-1} could be ascribed to the bending vibration of SO_4^{2-} [38]. To further reveal the effect of PDDA on Zn surface, the bending vibration of –C–N (PDDA) was carefully measured (Fig. 1e). Pure

PDDA has two obvious peaks, which correspond to stretching and shear vibration [37]. However, when PDDA is absorbed on Zn surface ($ZnSO_4$-0.8% PDDA), the merge of two distinct peaks into one single peak indicates a strong interaction between PDDA and Zn in terms of molecule vibration modes. XPS result further proves the interaction between PDDA and Zn (Figs. 1f, S1c). The characteristic peak at N 1s orbital has shifted from 400.8 (pure PDDA) to 402.0 eV (PDDA on Zn anode surface), which indicates that quaternary ammonium ion can interact with Zn metal [39–41].

To further explain the action mechanism of PDDA, the PDDA unit was chosen as a research object. Density functional theory (DFT) calculations were also used to confirm the interaction between PDDA and Zn. Model of DFT calculations of binding energy is shown in Fig. S1d. When PDDA unit and H_2O are absorbed on different Zn crystal planes (002), (101) and (102), binding energies of PDDA are consistently lower than those of H_2O, which implies that PDDA could be more easy absorpted on the surface of Zn anode. Furthermore, the binding energy of PDDA on Zn (002) plane is the lowest (Fig. 1g), indicating that PDDA has the strongest interaction between PDDA and Zn (002) plane. In other words, Zn (002) plane may be preserved during Zn plating/stripping process [42].

Owing to its cation-rich nature, PDDA, serving as an electrolyte additive, provides the potential to engineeringly controlled Zn^{2+} deposition by means of the intrinsic electrostatic shielding effect [1, 5, 43]. Model of DFT calculations of system energy is shown in Fig. 1h. The calculation model is a positively charged PDDA unit absorbed on Zn (002) plane, and Zn^{2+} continues to move closer to the Zn (002) plane. As a result of the same charge repulsion (PDDA unit and Zn^{2+}), the overall system energy would increase upon the addition of PDDA. When the distance from Zn^{2+} to Zn (002) plane is around 1.0–1.8 nm, system energies are about –16 eV either with or without PDDA. When the distance is around 0.4–0.8 nm, the system energy rapidly increases. When PDDA is present, it is coincided with the closer proximity of Zn^{2+} to Zn (002) plane. To the contrary, the system energy without PDDA remains almost constant. Consequently, PDDA can provide the electrostatic shielding effect for Zn^{2+} deposition. The electrostatic shielding effect also can inhibit the growth of Zn dendrite [44].

A three-electrode system was used to analyze the function of PDDA in electrolyte. Cyclic voltammetry (CV) measurements were carried out to study the effect of PDDA on the reversibility of Zn plating and stripping. As shown in Fig. 2a, the redox peaks of Zn plating and stripping shift to the lower left and the corresponding peak currents also decrease, when PDDA was added into the electrolyte. This indicates that PDDA slows down the rate of Zn plating and stripping. The chronoamperometry (CA) was used to further investigate the effects of PDDA additive on the Zn nucleation and growth (Fig. 2b) at − 150 mV (vs. Zn^{2+}/Zn). The initial current density of $ZnSO_4$-0.8% PDDA (absolute value) is less than that of $ZnSO_4$, and the current density increases until the first 6 s. A current rise (0–6 s) indicates that nucleation and growth enhance Zn metal electrode surface area of $ZnSO_4$ and $ZnSO_4$-0.8% PDDA. In the following process, the current of $ZnSO_4$ continues to increase, while the $ZnSO_4$-0.8% PDDA current decreases after 6 s, demonstrating that the deposition of Zn is restrained by PDDA in electrolyte. In addition, the Tafel plot was tested for the reduced corrosion current density of Zn electrode in $ZnSO_4$ and $ZnSO_4$-0.8% PDDA electrolytes (Fig. 2c). For aqueous electrolyte, hydrogen evolution corrosion often occurs. The corrosion current density of $ZnSO_4$ and $ZnSO_4$-0.8% PDDA is of 1.26 and 0.45 $mA{\cdot}cm^{-2}$, respectively. The incorporation of PDDA results in a decrease of the corrosion current, suppress of hydrogen evolution corrosion, as well as an improvement in the zinc anode's compatibility with the electrolyte. The corrosion potential decreases from − 1.005 to − 1.018 V (vs. SCE) with PDDA added. Moreover, the decrease in the corrosion potential also indicates the reduced propensity for hydrogen evolution, thereby providing evidence of corrosion inhibition.

To further verify the inhibitory effect of PDDA additives on Zn surface corrosion, Zn foils were soaked in $ZnSO_4$ and $ZnSO_4$-0.8% PDDA electrolytes for 7 days, respectively. The corresponding scanning electron microscope (SEM) images show the presence of many large angular particles on Zn foil surface when using $ZnSO_4$ electrolyte (Fig. 2d). However, a compact and flat Zn surface is maintained in the PDDA containing electrolyte (Fig. 2e). The soaked Zn foils were tested by X-ray diffraction (XRD). The emergence of reflections can be attributed to the newly formed by-products $Zn_4(OH)_6SO_4{\cdot}xH_2O$ (x = 0.5, 2, 4, 5 and 6, abbreviated as ZOSH) for the $ZnSO_4$ electrolyte, as shown in Fig. 2f. Many large angular particles (Fig. 2d) should be ZOSH by-products. The H_2 evolution and by-product formation are mainly ascribed to the Zn corrosion. It raises the local pH value and then triggers the precipitation reaction of OH^- with Zn^{2+}, SO_4^{2-}, and H_2O ($4Zn^{2+} + SO_4^{2-} + 6\ OH^- + xH_2O \rightarrow Zn_4(OH)_6SO_4{\cdot}xH_2O$). By contrast, only the characteristic peak of Zn is found for zinc foil soaked without other miscellaneous peaks, which implies that no by-products are produced in $ZnSO_4$-0.8% PDDA electrolyte (Fig. 2f). According to the DFT result, PDDA tends to be absorbed on Zn surface rather than H_2O, thereby protecting the Zn surface from corrosion of H^+ (from H_2O).

Considering that PDDA is a cation-rich polymer and easy to be adsorbed on Zn anode surface, Fig. 2g, h illustrates how electrostatic shielding effect inhibits the growth

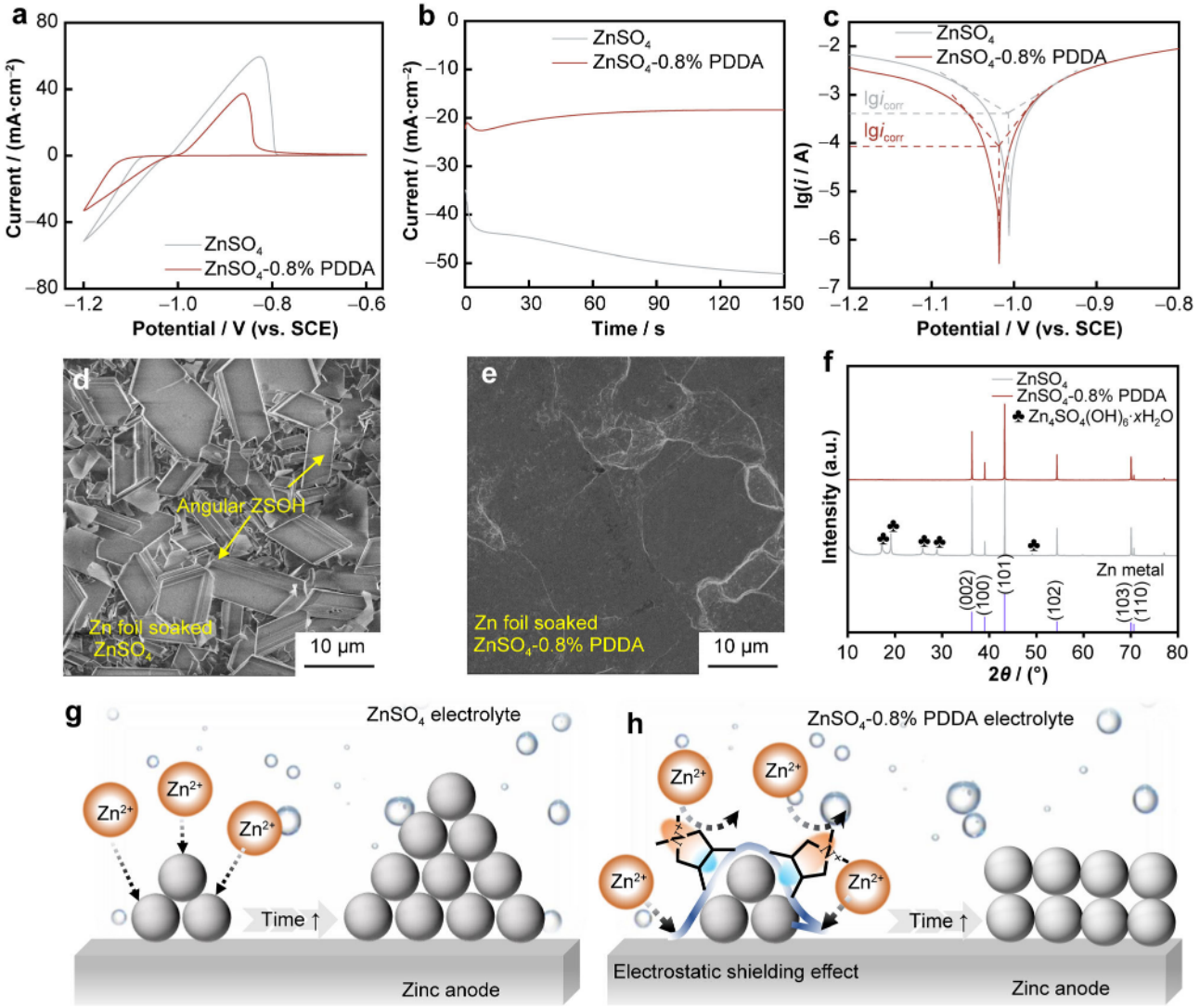

Fig. 2 Role of PDDA additive on Zn deposition: **a** CV curves in $ZnSO_4$ and $ZnSO_4$-0.8% PDDA, with Cu foil as a worker electrode; **b** chronoamperometric curves of Zn electrodeposition under − 150 mV; **c** Tafel plots of metal Zn in $ZnSO_4$ and $ZnSO_4$-0.8% PDDA; **d**, **e** SEM images and **f** XRD patterns of Zn foil soaked in $ZnSO_4$ and $ZnSO_4$-0.8% PDDA for 7 days; illustration of Zn deposition process based on electrostatic shielding effect **g** without PDDA and **h** with PDDA

of Zn dendrites. In conventional $ZnSO_4$ electrolytes, decomposition process of Zn inevitably leads to the formation of some protuberant tips. A strong electric field will be generated around protuberant tips, which accelerates the deposition of Zn and tends to form dendrites (Fig. 2g) [5]. In addition, the cation-rich PDDA polymer chain can produce strong electrostatic repulsion with Zn^{2+} in the electrolyte, which will restrain the growth of zinc dendrites even at protuberate tips (Fig. 2h).

2.2 Electrochemical performance of Zn||Zn cells

Through the study of a three-electrode system, it was found that PDDA had the ability to control the growth of Zn dendrites. To systematically assess the practical performance of PDDA additives to effectively inhibit the Zn dendrite growth, the Zn||Zn symmetric cells were assembled for electrochemical characterization. Electrochemical impedance spectroscopy (EIS) analysis is presented in Fig. 3a–c. Nyquist profiles (Fig. 3a) demonstrate that the diameter of impedance semicircle decreases with the addition of PDDA, indicating a decrease in charge transfer resistance (R_{ct}) (Table S1). The R_{ct} of cell with $ZnSO_4$-0.8% PDDA was the smallest among three samples. Similarly, the impedance magnitudes of cell in $ZnSO_4$-0.8% PDDA and $ZnSO_4$-1.6% PDDA are smaller than those in pure $ZnSO_4$ among all the frequency (Fig. 3b). The diffusion coefficient of Zn ions on the electrode surface can be estimated by linear fitting of the low-frequency part (0.1–0.01 Hz). Figure 3c shows three kinds of

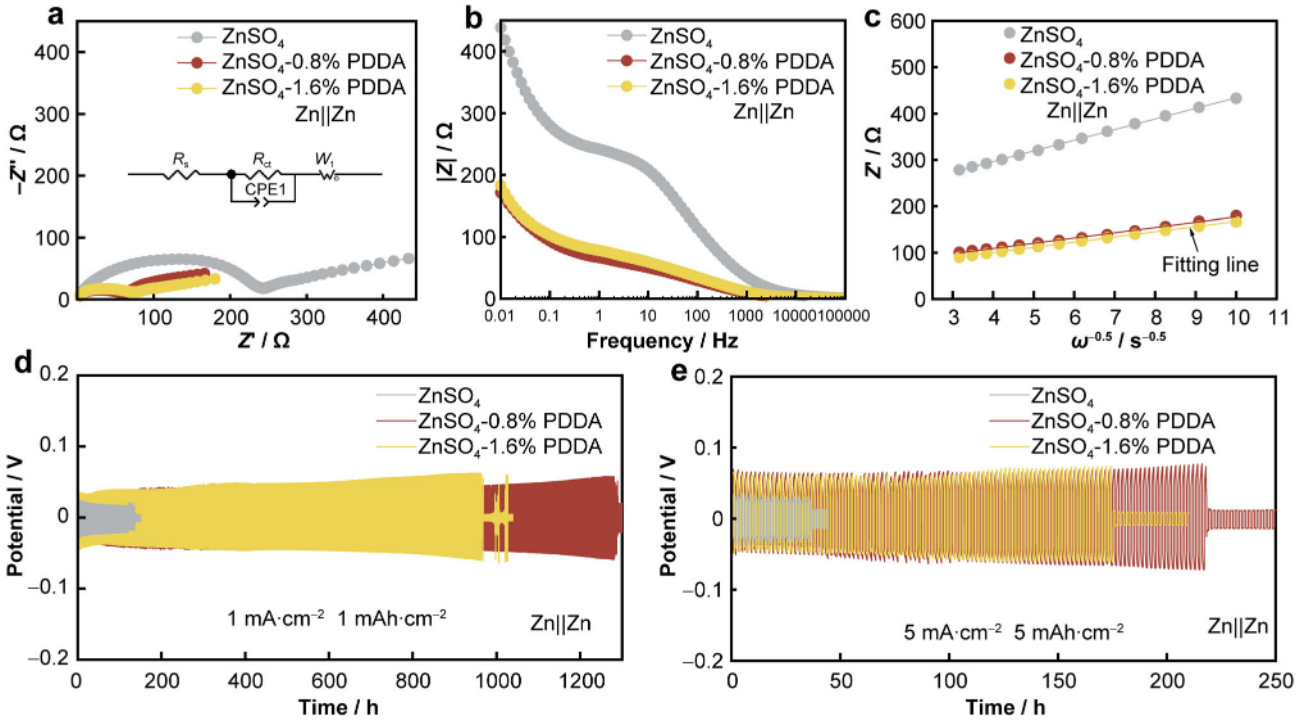

Fig. 3 Electrochemical performance of Zn||Zn symmetric battery in different electrolytes: **a** EIS plots before cycling and (inset) equivalent circuit, where R_s represents contact resistance, R_{ct} is charge transfer impedance, CPE is constant phase element, and Z_w is Warburg impedance; **b** Bode curve; **c** low-frequency linear fitting curve; galvanostatic zinc plating/stripping in Zn||Zn symmetric cells at **d** current density of 1 mA·cm ^{2} and areal capacity of 1 mAh·cm ^{2} and **e** 5 mA·cm ^{2} and 5 mAh·cm ^{2}

electrolytes with linear fitting. The slop (σ) of $ZnSO_4$-0.8% PDDA is almost equal to that of $ZnSO_4$-1.6% PDDA (Table S1). And their slop values are lower than those of $ZnSO_4$. According to Eqs. (S1–S3), diffusion coefficients (D) of $ZnSO_4$-0.8% PDDA and $ZnSO_4$-1.6% PDDA are higher than that of $ZnSO_4$, indicating that PDDA additive can improve properties of ions diffusion. However, PDDA additive increases the polarization of Zn metal anode, which is contradicted by EIS test (Fig. 2a). A reasonable explanation is that CV involved electrochemical reactions (i.e., Zn deposition), while EIS of Zn||Zn cell represented a physical process, without chemical reactions occurring. EIS is the movement of charge carriers in electric fields of different frequencies [45]. Owing to the presence of abundant positive charge carriers in PDDA and its adsorption on the surface of Zn anode, more charges were involved in the movement, which reduced internal resistance of Zn anode. According to the principle of electrostatic shielding effect, it takes place during the electrochemical process that regulates deposition of Zn^{2+} and enhances electrochemical polarization [25].

The plating/stripping test was conducted in Zn||Zn symmetric cells under different galvanostatic conditions to evaluate the electrochemical performance. As shown in Fig. 3d, e, the cycle life of Zn||Zn symmetric cells containing PDDA is substantially longer than that of symmetric cells with pure $ZnSO_4$. Among them, $ZnSO_4$-0.8% PDDA has the longest life span of over 1200 h, under 1 mA·cm^{-2} with 1 mAh·cm^{-2}. $ZnSO_4$-1.6% PDDA sample, which contains a high concentration of PDDA, has an extended lifetime of more than 900 h before short circuit occurs. The shortest life of $ZnSO_4$ is less than 150 h prior to short circuit. Note that the polarization potential of $ZnSO_4$ is about 39 mV, while the polarization potentials of cell in $ZnSO_4$-0.8% PDDA and $ZnSO_4$-1.6% PDDA are about 80 and 83 mV, respectively, during the initial process. The main reason for this phenomenon can be that PDDA regulates Zn deposition and restrains the growth of Zn dendrites via electrostatic shielding effect of PDDA, which is consistent with Fig. 2a, b. Many cations enhance the electrostatic shielding effect, but result in increased polarization. In this case, the polarization potentials of $ZnSO_4$-1.6% PDDA is greater than those of $ZnSO_4$-0.8% PDDA, which is detrimental to the suppression of Zn dendrites growth. When the test condition was changed to high current (5 mA·cm^{-2}), the advantage of PDDA additive exhibits more obviously (Fig. 3e). $ZnSO_4$-0.8% PDDA has the longest life span of over 200 h, while $ZnSO_4$-1.6% PDDA has a lifespan of 144 h. $ZnSO_4$ has a shortest cycle of only 40 h. Therefore, it is worthwhile to explore $ZnSO_4$-0.8% PDDA in the next step.

The rate performance of the symmetric cells was studied with fixed 30 cycles. The area capacity of 1 mAh·cm^{-2} at current densities of 1, 2, 5, 10 and 30 mA·cm^{-2} (Fig. 4a). The overall polarization of $ZnSO_4$-0.8% PDDA is higher than that of $ZnSO_4$, which is consistent with previous testing. The symmetric cell in pure $ZnSO_4$ tends to suffer from short circuit after 120 h, while $ZnSO_4$-0.8% PDDA maintains good cycle stability due to the suppression of Zn dendrite growth. As shown in Fig. 4b, when the cell was tested at 5 mA·cm^{-2} and 1 mAh·cm^{-2}, the cell of $ZnSO_4$ could last only 62 h, while the life of $ZnSO_4$-0.8% PDDA was extended to more than 280 h. To further reveal the failure process of $ZnSO_4$, the cycled Zn electrodes were characterized by XRD and SEM after cycling for 62 h (Fig. 4c–e). There appears ZOSH reflections for $ZnSO_4$ (Fig. 4c), but they are absent in $ZnSO_4$-0.8% PDDA. During the process of Zn deposition, H_2 was generated, resulting in high pH near the electrode. With higher pH, ZOSH is easier to be formed on the electrode surface in the pure $ZnSO_4$ electrolyte. Based on three-electrode test and immersion experiment (Fig. 2), PDDA additive can observed to effectively inhibit the generation of H_2 and ZOSH. Therefore, Zn anode exhibits reduced propensity for the formation of ZOSH in the $ZnSO_4$-0.8% PDDA electrolyte. In addition, Zn metal anode has loose and uneven surface, leading to lamellar dendrites on the electrode surface in pure $ZnSO_4$ electrolyte (Fig. 4d). Owing to the electrostatic shielding effect of PDDA, a highly compact and dendrite-free surface is presented in Fig. 4e under the same condition.

According to DFT results, PDDA tends to be adsorbed on the Zn (002) plane, preserving the crystal plane of (002)

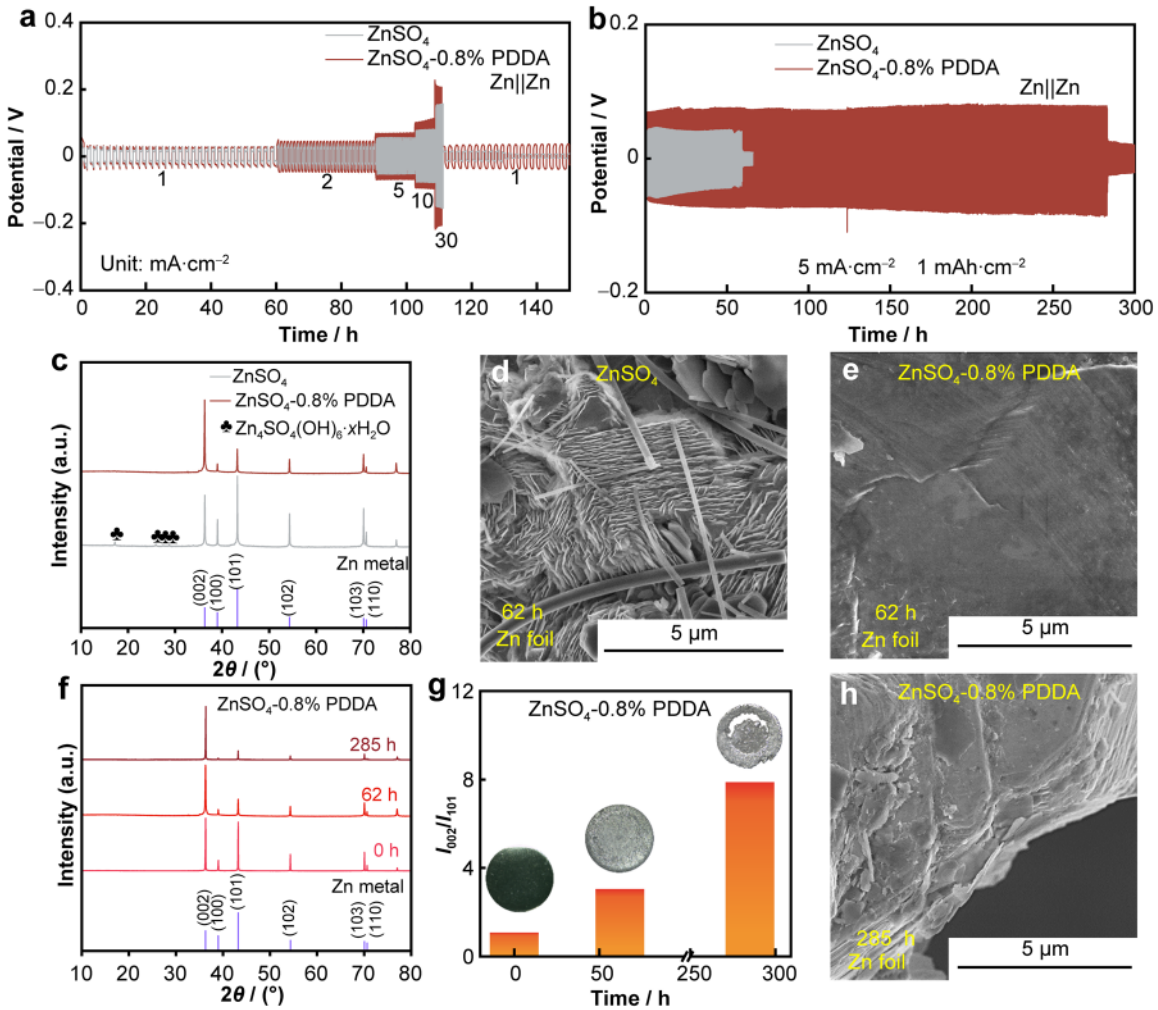

Fig. 4 Electrochemical performances of Zn||Zn symmetric cells in $ZnSO_4$ and $ZnSO_4$-0.8% PDDA electrolytes: rate performance at different current densities with an area capacity of **a** 1 mAh·cm ^{2} and **b** 5 mA·cm ^{2} and 1 mAh·cm ^{2}; **c** XRD patterns of Zn metal anode after cycling for 62 h at current densities of 5 mA·cm ^{2} and 1 mAh·cm ^{2}; SEM images of Zn metal anode after cycling for **d** $ZnSO_4$ and **e** $ZnSO_4$-0.8% PDDA for 62 h; **f** XRD patterns of Zn metal anode after cycling for different times; **g** I_{002}/I_{101} of Zn metal anode; and **h** SEM image of Zn foil in $ZnSO_4$-0.8% PDDA after 280 h

upon the Zn plating/stripping process. The growth of dendrites can be largely avoided when Zn metal is mainly deposited on (002) crystal plane [42]. XRD patterns of Zn metal anode were tested after cycling for 0, 62 and 285 h for $ZnSO_4$-0.8% PDDA electrolyte, respectively (Fig. 4f). The relative intensity of Zn (101) plane gradually decreased with operating time extending. XRD intensity is positively correlated with the number of crystal planes. The relative peak intensity of (002) over (101), denoted as I_{002}/I_{101}, indicates the relative amount of (002) plane for Zn anode (Fig. 4g). The value of I_{002}/I_{101} continues to increase from 0 to 285 h (failure time), confirming the (002) plane dominated upon Zn deposition, which is consistent with DFT results. However, Fig. 4g inset shows Zn anode perforated after a long cycle, which might lead to the failure of Zn||Zn symmetric cells. Figures 4h, S2 both show that Zn foil was severely perforated. Lots of steps appeared and Zn dendrites were absent, which could be attributed to a typical plane type growth due to the electrostatic shielding effect. At the same time, PDDA would also bring perforation of Zn anode issue.

2.3 Electrochemical performance of Cu||Zn and foamy Cu–Zn||foamy Cu–Zn cells

Considering that PDDA additive can effectively restrain the growth of Zn dendrites, when the intrinsic perforation issue brought from PDDA can be settled mildly, it is useful to optimize electrochemical performance via composite anodes technique.

The first step is to combine Cu with Zn anode to solve the perforation issue, due to the better chemical stability of Cu than that of Zn. Figure 5a–c shows the electrochemical performances of asymmetric cells (Cu||Zn) in $ZnSO_4$ and $ZnSO_4$-0.8% PDDA. The configuration of Cu||Zn cell is shown in the inset image (Fig. 5a). The test condition is charging cutoff potential of 0.5 V (vs. Zn^{2+}/Zn), discharging cutoff capacity of 0.5 mAh·cm^{-2} and current density of 0.5 mA·cm^{-2}. It is worth mentioning that Coulombic efficiency (CE) of $ZnSO_4$-0.8% PDDA is higher than that of $ZnSO_4$, especially during the initial cycles, which indicates that PDDA additive facilitates Zn plating/stripping on Cu foil surface and improves the electrochemical reversibility (Fig. 5a). In subsequent cycles, $ZnSO_4$-0.8% PDDA CE gradually approaches 100%. Figure S3a, b shows the voltage profiles of the 1st and 20th cycles, respectively. The charge capacity of $ZnSO_4$-0.8% PDDA is superior to that of $ZnSO_4$ in the 1st cycle. Furthermore, Cu|$ZnSO_4$-0.8% PDDA|Zn has a much better cycle life than Cu|$ZnSO_4$|Zn, as shown in Fig. S3c.

In the next step, the current and capacity of Cu||Zn cells were set to the same condition as the above-measured Zn||Zn cell (5 mA·cm^{-2} and 1 mAh·cm^{-2}). Figure S4a shows Cu||Zn cells plating/stripping cycle life. When cycling time was around 64 h, short circuit occurred in the Cu||Zn employing $ZnSO_4$. However, the Cu||Zn cell had a lifetime of over 1000 h in $ZnSO_4$-0.8% PDDA electrolyte, which was far more than the Zn||Zn cell (Fig. 4b) under the same conditions. Cu foil in $ZnSO_4$ and $ZnSO_4$-0.8% PDDA electrolytes after cycling for 64 h was further analyzed by SEM. Lamellar dendrites are observed on the Cu surface for $ZnSO_4$ (Fig. 5b), whereas Cu foil has a flat dendrite-free surface in $ZnSO_4$-0.8% PDDA electrolyte (Fig. 5c). This phenomenon can be ascribed to the electrostatic shielding effect of PDDA.

However, normal Cu foil is unsuitable for direct use as an anode due to the lack of Zn^{2+} supply. Furthermore, if Zn foil is covered with copper foil as a composite anode, a copper foil does not effectively facilitate the penetration of Zn^{2+} from copper foil to Zn foil. Therefore, a porous and foamy Cu–Zn composite anode was introduced. The structure of foamy Cu–Zn anode is shown in the inset image (Fig. 5d). The symmetric cell was tested by the condition of 5 mA·cm^{-2} and 1 mAh·cm^{-2} and $ZnSO_4$-0.8% PDDA served as the electrolyte. The curve displays a symmetric shape, which is a typical characteristic observed in symmetric cell (Figs. 5d, S5a, b). The foamy Cu–Zn symmetric cell has a prolonged lifetime of over 1200 h, which is much longer than the Zn symmetrical cell life (Fig. 4b) under the same testing condition.

Figures 5e, S5c show the pristine and cycled (1200 h) optical images of foamy Cu and Zn foil in light transmittance and reflectance. Pristine foamy Cu presents the porous structure, while pristine Zn foil is a piece of continuous solid. After 1200 h cycling, the pores of foamy Cu were filled with zinc metal, while the Zn foil was perforated. In other words, zinc metal was gradually transferred to foamy Cu during zinc plating/stripping process. SEM images of foamy Cu of $ZnSO_4$-0.8% PDDA before and after cycling are shown in Fig. 5f–g. The pristine foamy Cu is frame-like (Fig. 5f).

Figure 5g also presents the SEM image of foamy Cu–Zn symmetric cells in $ZnSO_4$-0.8% PDDA after 1200 h. The voids of foamy Cu have been filled with Zn metal. Zn deposition on the surface of foamy Cu is relatively flat without the growth of Zn dendrites, as shown in Fig. 5h. Moreover, XRD patterns further verify the above-mentioned phenomenon (Fig. S5d). Pristine foamy Cu exhibits only three main reflections without impurity. After 1200-h cycling, XRD presents strong zinc characteristic peaks. There is an orientation on Zn (002) plane, which indicates that the preferential growth of Zn within foam Cu foil occurred due to the influence of PDDA additive. When foamy Cu was combined with Zn foil, Zn foil was perforated upon cycling. XRD patterns of Zn reveal the absence of preferential growth along the (002) plane, and newly

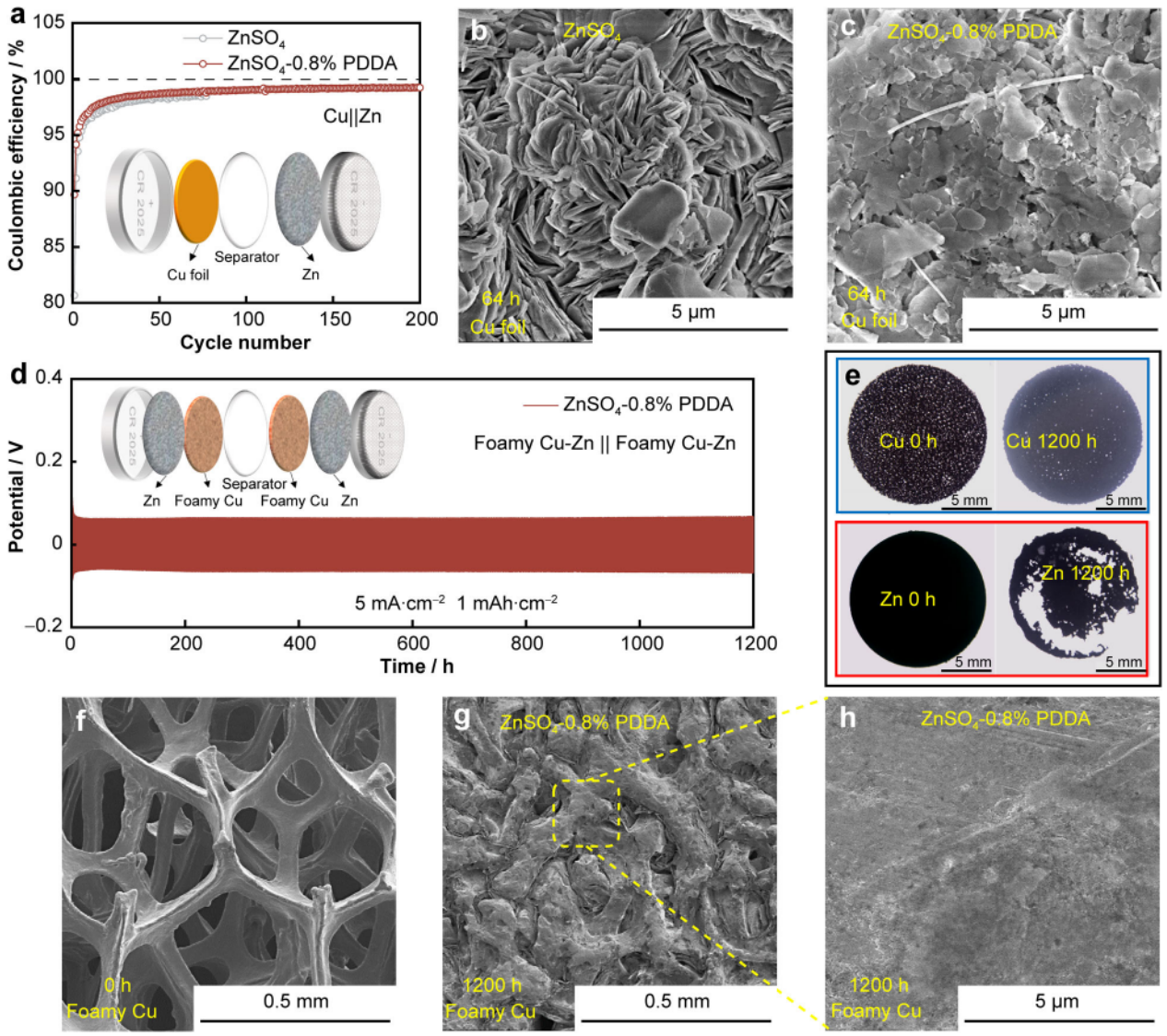

Fig. 5 Electrochemical performance of asymmetric Cu||Zn cells in $ZnSO_4$ and $ZnSO_4$-0.8% PDDA: **a** Coulombic efficiency under charging cutoff potential of 0.5 V (vs. Zn^{2+}/Zn) and discharging cutoff capacity of 0.5 mAh·cm ^{2}; SEM images of Cu foil in **b** $ZnSO_4$ and **c** $ZnSO_4$-0.8% PDDA electrolytes after 64 h under 5 mA·cm ^{2} and 1 mAh·cm ^{2}. Electrochemical performance of foamy Cu–Zn symmetric cells in $ZnSO_4$-0.8% PDDA electrolyte at current densities of 5 mA·cm ^{2} and 1 mAh·cm ^{2}: **d** cycling performance of cells; **e** optical photographs of foamy Cu and Zn foil before and after cycling; SEM images of foamy Cu in $ZnSO_4$-0.8% PDDA electrolyte **f** before and **g**, **h** after cycling

formed reflections can be attributed to ZOSH by-product on the Zn foil (Fig. S5e). Therefore, the introduction of foamy Cu–Zn electrode can successfully solve the issue of Zn foil perforation during plating/stripping process. Meanwhile, Zn^{2+} disposition and dendrite growth are also inhibited by PDDA for the foamy Cu–Zn electrode.

2.4 Cycling performance of Zn-ion supercapacitors (ZHCs) and Zn-ion cells

To explore the potential application of PDDA additives, Zn-ion hybrid supercapacitors (ZHCs) have been assembled with commercial active carbon (AC) as a cathode, and foamy Cu–Zn as an anode in the $ZnSO_4$-0.8% PDDA and $ZnSO_4$ electrolytes, respectively. CV curves show a quasi-rectangular shape with reversible redox humps at various scan speeds, which is basically the combination of capacitor and battery behavior for $ZnSO_4$-0.8% PDDA and $ZnSO_4$ (Figs. 6a, S6a). Zn ions were reversibly absorbed/desorbed on AC cathode (capacitor behavior), while Zn plating/stripping process happened on the foamy Cu–Zn anode (battery behavior), which widens the potential window and improves the capacity. CV area of ZHC with $ZnSO_4$-0.8% PDDA is generally larger than

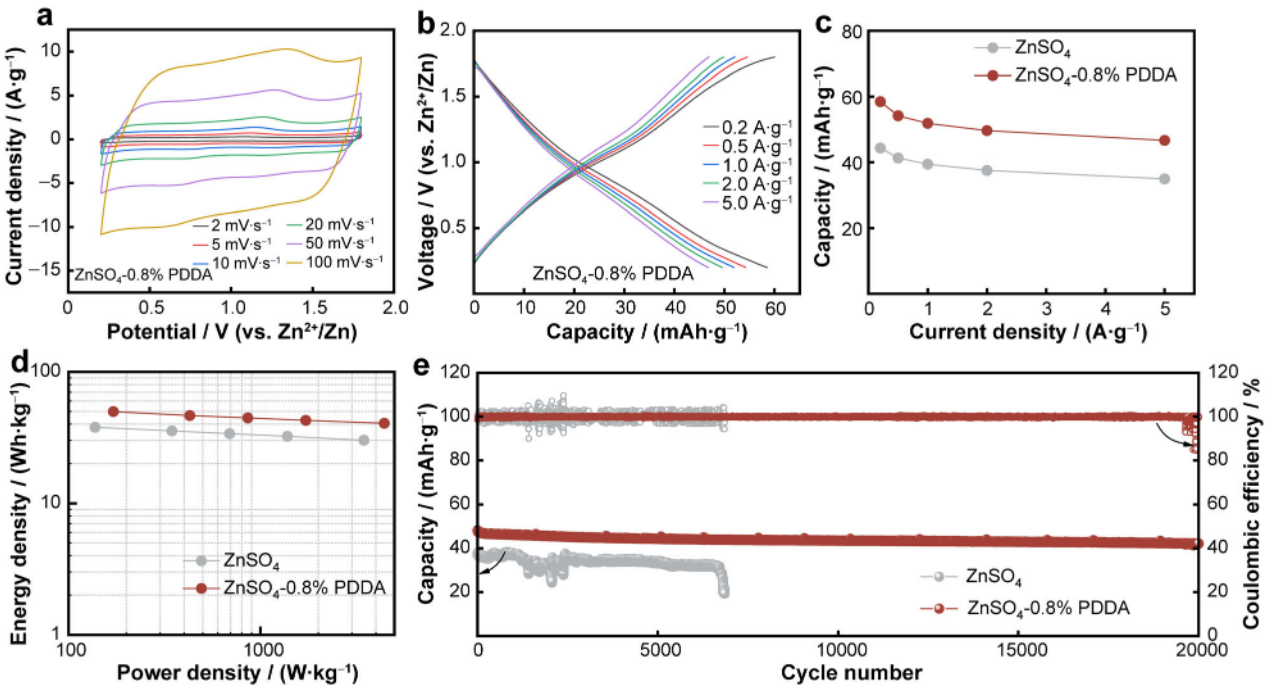

Fig. 6 Electrochemical performance of Zn-ion hybrid supercapacitors (ZHCs) in $ZnSO_4$ and $ZnSO_4$-0.8% PDDA electrolytes: **a** CV curves at different scan rates; **b** GCD profiles at different current densities; **c** rate performance test; **d** Ragone plot based on mass loading of cathode active material; and **e** cycling performance at a current density of 5 A·g ^{1}

that of $ZnSO_4$ (Figs. 6a, S6a) at different scan speeds, signifying that the capacity is higher when $ZnSO_4$-0.8% PDDA is used as the electrolyte. Galvanostatic charge–discharge (GCD) is a direct measure in terms of capacity. In Figs. 6b, S6b, GCD curves of ZHC in $ZnSO_4$-0.8% PDDA and $ZnSO_4$ were nearly symmetric at different current density (0.2–5 $A{\cdot}g^{-1}$), indicating a typical capacitor for AC cathode. Moreover, capacities of ZHCs in $ZnSO_4$ and $ZnSO_4$-0.8% PDDA at different current density (0.2–5 $A{\cdot}g^{-1}$) are shown in Fig. 6c. The ZHC in $ZnSO_4$-0.8% PDDA always delivers higher capacities in $ZnSO_4$. The possible reason is that PDDA contains smaller ionic radius Cl^- and improves capacitance. Thus, energy density of ZHC in $ZnSO_4$-0.8% PDDA is correspondingly higher than that of $ZnSO_4$ (Fig. 6d) at different power densities. Regarding long GCD cycling test, PDDA additive exerts a huge advantage (Fig. 6e). The capacity of $ZnSO_4$ was 38.8 $mAh{\cdot}g^{-1}$ in the first 10 cycles. With cycle number increasing, CE becomes unstable in $ZnSO_4$, which implies that the side reactions are exacerbated in ZHCs. The capacity rapidly decreases to 19.8 $mAh{\cdot}g^{-1}$ after 6850 cycles, which is only 51% of the capacity in the 10th cycle, indicating that slight short-circuit ZHCs occurred and the growth of Zn dendrites on Zn anode began. For the purpose of demonstrating short circuit taking place, ZHCs were dismantled after the loop for 6850 cycles, and surface morphology tests were conducted on the foamy Cu. The surface of foamy Cu of $ZnSO_4$ exhibits severe dendritic growth (Fig. S6c). On the contrary, the surface of foamy Cu of $ZnSO_4$-0.8% PDDA displays a smooth and flat appearance as shown in Fig. S6d. When PDDA is added into electrolyte and foamy Cu–Zn is used as anode, the capacity of ZHC with the $ZnSO_4$-0.8% PDDA electrolyte is of 44.5 $mAh{\cdot}g^{-1}$ in the first 10 cycles. The capacity maintains stable in subsequent cycles and is of 39.5 $mAh{\cdot}g^{-1}$ in the 20000th cycle with a capacity retention of 89%.

In addition, note that PDDA additive is also suitable for MnO_2||Zn cells. MnO_2||Zn cells were assembled by MnO_2 as a cathode, Zn foil as an anode with $ZnSO_4$–$MnSO_4$-0.8% PDDA electrolyte. MnO_2 cathode was prepared by hydrothermal method, and its morphology shows an acicular shape (Fig. S7a). XRD pattern matches with the standard (JCPDS No. 44-0142) (Fig. S7b). Furthermore, the addition of a certain amount of $MnSO_4$ into electrolyte can inhibit dissolution of MnO_2 upon cycling to improve cycling performance. To reveal the redox behavior of MnO_2||Zn cells, CV were measured and the curves displayed significant redox peaks [46]. Upon reduction, there appeared two distinct reduction peaks, which represented the insertion of H^+ and Zn^{2+} into MnO_2. In the oxidation process, a main oxidation peak and an accompanying peak appeared, indicating the de-insertion of H^+ and Zn^{2+}. Regarding CV measurements, redox peaks have slightly pronounced in the $ZnSO_4$–$MnSO_4$-0.8% PDDA electrolyte, which indicates PDDA additive enhances the capacity of

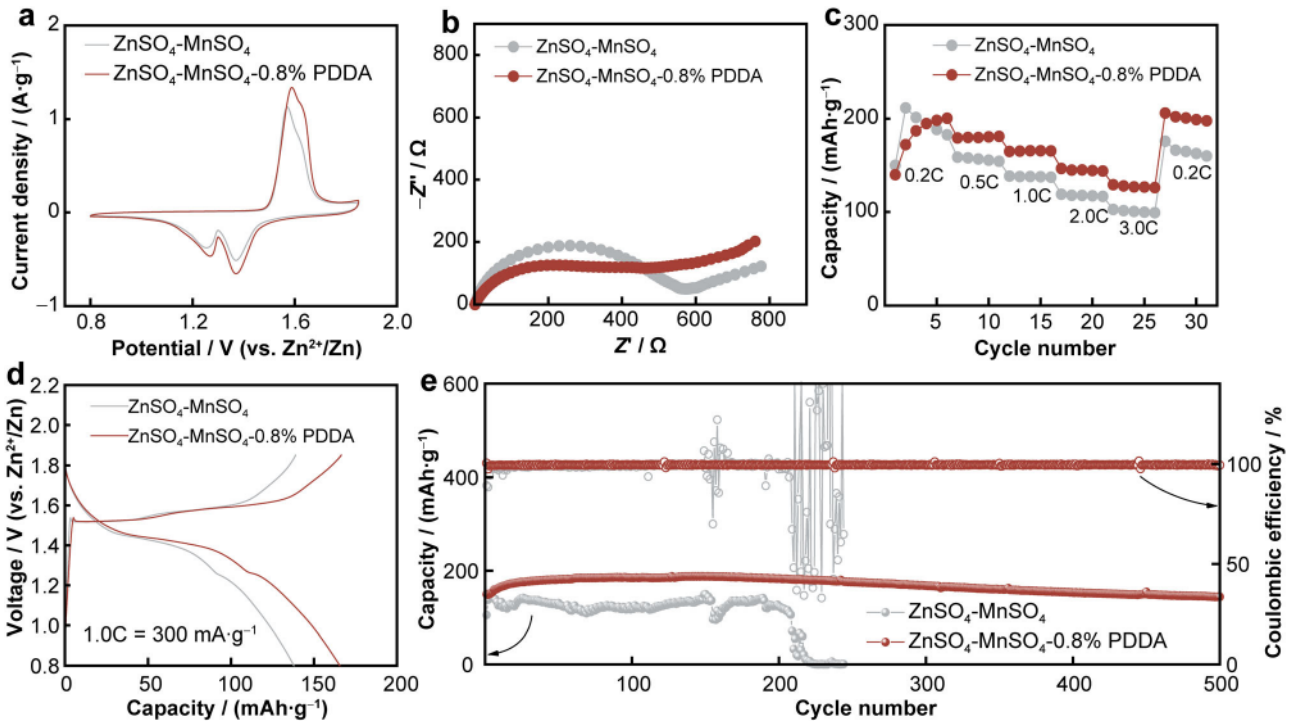

Fig. 7 Electrochemical performance of MnO_2||Zn cells in $ZnSO_4$ and $ZnSO_4$-0.8% PDDA electrolytes: **a** CV curves at scan rate of 0.2 mV·s ^{1}; **b** EIS plots; **c** rate performance; **d** GCD profiles under 1C; and **e** cycling performance at 2C

cathode EIS result shows that R_{ct} of cell in $ZnSO_4$–$MnSO_4$-0.8% PDDA is smaller than that of $ZnSO_4$–$MnSO_4$ (Fig. 7b), which is in line with the result of Zn||Zn symmetric cell (Fig. 3a). The cell delivered a higher capacity of $ZnSO_4$–$MnSO_4$-0.8% PDDA than that of the $ZnSO_4$–$MnSO_4$, independent of different current density (Fig. 7c). The discharge capacity increased with cycles going on, which typically follows a battery activation [46]. The advantage of PDDA additive is more obvious, particularly at current density of 2C and 3C (1C = 300 mA·g^{-1}). It can be attributed to Cl^- involvement of enhanced activity of MnO_2 [47]. MnO_2||Zn cells displayed two plateaus upon discharge, implying co-intercalation of Zn^{2+} and H^+ separately. However, voltage profiles of the identical cell configuration only show one charge plateau (Fig. 7d). These plateaus well correspond to redox peaks of CV (Fig. 7a). When the cell was operated galvanostatically at 2C for long-term cycling test, it exhibited much longer cycle life with $ZnSO_4$–$MnSO_4$-0.8% PDDA than the ones without PDDA (Fig. 7e). The initial discharge capacity was about 158 mAh·g^{-1}. Its capacity increased gradually to around 200 mAh·g^{-1} in the 100th cycle. This might be caused by the catalytic process of MnO_2 upon cycling. And it remains 144 mAh·g^{-1} in the 500th cycle with a capacity retention of 91.1%. For battery with $ZnSO_4$–$MnSO_4$ electrolyte, the initial capacity was 150 mAh·g^{-1}, which was comparable to $ZnSO_4$–$MnSO_4$-0.8% PDDA. However, $ZnSO_4$–$MnSO_4$ capacity started decreasing from the 181st cycle, and meanwhile, the CE was also unstable. The capacity of cell in the $ZnSO_4$–$MnSO_4$ electrolyte fell to nearly zero in the 250th cycle, due to the unwanted reaction at the Zn anode and short circuit caused by Zn dendrites. In this case, it can recertify that PDDA was absorbed on Zn (002) plane, and corresponding electrostatic shielding effect could effectively inhibit by-products and restrain the growth of Zn dendrites.

3 Conclusion

Summing up, a cationic polymer PDDA was introduced as an effective additive to stabilize Zn anode. PDDA, absorbed preferentially on Zn (002) plane, not only provides an electrostatic shielding effect to restrain the growth of Zn dendrites, but also protects Zn anode from side reaction. Furthermore, to mitigate the issue of Zn electrode perforation caused by PDDA additive, a successful approach was introduced by combining more chemically stable foamy copper with Zn foil. With the PDDA additives in electrolyte, Zn anode life is more than 1100 h in the Zn||Zn cell (1 mA·cm^{-2} and 1 mAh·cm^{-2}). In addition, Zn-ion hybrid supercapacitors (ZHCs) and MnO_2||Zn batteries with PDDA additive exhibit excellent rate performance and durable lifespans. ZHCs and MnO_2||Zn batteries

life reach 20,000 cycles and 500 cycles, respectively. Our findings might lead to a simple and effective engineering strategy for inhibiting the formation of metal dendrite, allowing Zn-ion batteries and Zn-ion supercapacitors to have a long cycle life in potential applications.

Acknowledgements This work was financially supported by Fuzhou science and technology project (Nos. 2021-ZD-213 and 2020-Z-6), Fujian Provincial Department of Science and Technology (Nos. 2021T3036, 2020T3004, 2020T3030 and 2020H0040), STS Science And Technology Project of the Chinese Academy of Sciences (No. KFJ-STS-QYZD-2021-09-001), Quanzhou Science and Technology Project (No. 2020G17), and the Joint Fund of the Yulin University and the Dalian National Laboratory for Clean Energy (No. 2021009).

Declarations

Conflict of interests The authors declare that they have no conflict of interest.

References

[1] Yao R, Qian L, Sui YM, Zhao GY, Guo RS, Hu SY, Liu P, Zhu HJ, Wang FC, Zhi CY, Yang C. A versatile cation additive enabled highly reversible zinc metal anode. Adv Energy Mater. 2021;12(2):2102780. https://doi.org/10.1002/aenm.202102780.

[2] Zhong C, Liu B, Ding J, Liu XR, Zhong YW, Li Y, Sun CB, Han XP, Deng YD, Zhao NQ, Hu WB. Decoupling electrolytes towards stable and high-energy rechargeable aqueous zinc-manganese dioxide batteries. Nat Energy. 2020;5(6):440. https://doi.org/10.1038/s41560-020-0584-y.

[3] Zhang N, Cheng FY, Liu JX, Wang LB, Long XH, Liu XS, Li FJ, Chen J. Rechargeable aqueous zinc-manganese dioxide batteries with high energy and power densities. Nat Commun. 2017;8(1):405. https://doi.org/10.1038/s41467-017-00467-x.

[4] Qian L, Yao WT, Yao R, Sui YM, Zhu HJ, Wang FC, Zhao JW, Zhi CY, Yang C. Cations coordination-regulated reversibility enhancement for aqueous Zn-ion battery. Adv Funct Maters. 2021;31(40):2105736. https://doi.org/10.1002/adfm.202105736.

[5] Nie XY, Miao LC, Yuan WT, Ma GQ, Di SL, Wang YY, Shen SG, Zhang N. Cholinium cations enable highly compact and dendrite-free Zn metal anodes in aqueous electrolytes. Adv Funct Mater. 2022;32(32):2203905. https://doi.org/10.1002/adfm.202203905.

[6] Yang Q, Liang GJ, Guo Y, Liu ZX, Yan BX, Wang DH, Huang ZD, Li XL, Fan J, Zhi CY. Do zinc dendrites exist in neutral zinc batteries: a developed electrohealing strategy to in situ rescue in-service batteries. Adv Mater. 2019;31(43):1903778. https://doi.org/10.1002/adma.201903778.

[7] Wang DH, Li Q, Zhao YW, Hong H, Li HF, Huang ZD, Liang GJ, Yang Q, Zhi CY. Insight on organic molecules in aqueous Zn-ion batteries with an emphasis on the Zn anode regulation. Adv Energy Mater. 2022;12(9):2102707. https://doi.org/10.1002/aenm.202102707.

[8] Gan Y, Wang C, Li JY, Zheng JJ, Wang HZ, Wang H. Stability optimization strategy of aqueous zinc ion batteries. Chin J Rare Met. 2022;46(6):753. https://doi.org/10.13373/j.cnki.cjrm.XY21100036.

[9] Liu GL, Zhang T, Li XJ, Cao RP, Shen JK, Guo DL, Wu NT, Yuan WW, Cao A, Liu XM. Oxygen-deficient ammonium vanadate/GO composites with suppressed vanadium dissolution for ultra-stable high-rate aqueous zinc-ion batteries. Rare Met. 2023;42(11):3729. https://doi.org/10.1007/s12598-023-02364-3.

[10] Zhu ZX, Lin ZW, Sun ZW, Zhang PX, Li CP, Dong R, Mi HW. Deciphering H^+/Zn^{2+} co-intercalation mechanism of MOF--derived 2D MnO/C cathode for long cycle life aqueous zinc-ion batteries. Rare Met. 2022;41(11):3729. https://doi.org/10.1007/s12598-022-02088-w.

[11] Zhao ZM, Zhao JW, Hu ZL, Li JD, Li JJ, Zhang YJ, Wang C, Cui GL. Long-life and deeply rechargeable aqueous Zn anodes enabled by a multifunctional brightener-inspired interphase. Energ Environ Sci. 2019;12(6):1938. https://doi.org/10.1039/C9EE00596J.

[12] Zhou JH, Xie M, Wu F, Mei Y, Hao YT, Li L, Chen RJ. Encapsulation of metallic Zn in a hybrid MXene/Graphene aerogel as a stable Zn anode for foldable Zn-ion batteries. Adv Mater. 2022;34(1):2106897. https://doi.org/10.1002/adma.202106897.

[13] Li B, Xue J, Lv X, Zhang RC, Ma KX, Wu XW, Dai L, Wang L, He ZX. A facile coating strategy for high stability aqueous zinc ion batteries: porous rutile nano-TiO_2 coating on zinc anode. Sur Coat Tech. 2021;421(15):127367. https://doi.org/10.1016/j.surfcoat.2021.127367.

[14] He HB, Tong H, Song XY, Song XP, Liu J. Highly stable Zn metal anodes enabled by atomic layer deposited Al_2O_3 coating for aqueous zinc-ion batteries. J Mater Chem A. 2020;8(16):7836. https://doi.org/10.1039/D0TA00748J.

[15] Yang Y, Liu CY, Lv ZH, Yang H, Zhang YF, Ye MH, Chen LB, Zhao JB, Li CC. Synergistic manipulation of Zn^{2+} ion flux and desolvation effect enabled by anodic growth of a 3D ZnF_2 matrix for long-lifespan and dendrite-free Zn metal anodes. Adv Mater. 2021;33(11):2007388. https://doi.org/10.1002/adma.202007388.

[16] An YL, Tian Y, Liu CK, Xiong SL, Feng JK, Qian YT. Rational design of sulfur-doped three-dimensional $Ti_3C_2T_x$ MXene/ZnS heterostructure as multifunctional protective layer for dendrite-free zinc-ion batteries. ACS Nano. 2021;15(9):15259. https://doi.org/10.1021/acsnano.1c05934.

[17] Jia H, Qiu MH, Lan CT, Liu HQ, Dirican M, Fu SH, Zhang XW. Advanced zinc anode with nitrogen-doping interface induced by plasma surface treatment. Adv Sci. 2022;9(3):2103952. https://doi.org/10.1002/advs.202103952.

[18] Ma LT, Zhi CY. Zn electrode/electrolyte interfaces of Zn batteries: a mini review. Electrochem Commun. 2021;122:106898. https://doi.org/10.1016/j.elecom.2020.106898.

[19] Xu CX, Jiang JJ. Electrolytes speed up development of zinc batteries. Rare Met. 2021;40(4):3. https://doi.org/10.1007/s12598-020-01628-6.

[20] Lin XS, Wang ZR, Ge LH, Xu JW, Ma WQ, Ren MM, Liu WL, Yao JS, Zhang CB. Electrolyte modification for long-life Zn ion batteries: achieved by methanol additive. ChemElectroChem. 2022;9(4):e202101724. https://doi.org/10.1002/celc.202101724.

[21] Eric H, Li HZ, Adulhakem YE. Rechargeable Zn^{2+}/Al^{3+} dual-ion electrochromic device with long life time utilizing dimethyl sulfoxide (DMSO)-nanocluster modified hydrogel electrolytes. RSC Adv. 2019;9(55):32047. https://doi.org/10.1039/C9RA06785J.

[22] Miao LC, Wang RH, Di SL, Qian ZF, Zhang L, Xin WL, Liu MY, Zhu ZQ, Chu SQ, Du Y, Zhang N. Aqueous electrolytes with hydrophobic organic cosolvents for stabilizing zinc metal anodes. ACS Nano. 2022;16(2):9667. https://doi.org/10.1021/acsnano.2c02996.

[23] Tran TNT, Zhao MS, Geng SJ, Ivey DG. Ethylene glycol as an antifreeze additive and corrosion inhibitor for aqueous zinc-ion batteries. Batteries Supercaps. 2022;5(6):e202100420. https://doi.org/10.1002/batt.202100420.

[24] Zhang SJ, Hao JN, Luo D, Zhang PF, Zhang BK, Davey K, Lin Z, Qiao SZ. Dual-function electrolyte additive for highly reversible Zn anode. Adv Energy Mater. 2021;11(37):2102010. https://doi.org/10.1002/aenm.202102010.
[25] Xu YT, Zhu JJ, Feng JZ, Wang Y, Wu XX, Ma PJ, Zhang X, Wang GZ, Yan XB. A rechargeable aqueous zinc/sodium manganese oxides battery with robust performance enabled by Na_2SO_4 electrolyte additive. Energy Storage Mater. 2021;38: 299. https://doi.org/10.1016/j.ensm.2021.03.019.
[26] Zheng XY, Zhou Y, Yan X, Lam KH, Hou XH. Vanadium oxide with elevated interlayers for durable aqueous hybrid Li^+/Zn^{2+} batteries. ACS Appl Energy Mater. 2022;5(7):9070. https://doi.org/10.1021/acsaem.2c01512.
[27] Tian M, Liu CF, Zheng JQ, Jia XX, Jahrman EP, Seidler GT, Long DH, Atif M, Alsalhi M, Cao GZ. Structural engineering of hydrated vanadium oxide cathode by K^+ incorporation for high-capacity and long-cycling aqueous zinc ion batteries. Energy Storage Mater. 2020;29:9. https://doi.org/10.1016/j.ensm.2020.03.024.
[28] Han DL, Wang ZX, Lu HT, Li H, Cui CJ, Zhang ZC, Sun R, Geng CN, Liang QH, Guo XX, Mo YB, Zhi X, Kang FY, Weng Z, Yang QH. A self-regulated interface toward highly reversible aqueous zinc batteries. Adv Energy Mater. 2022;12(9):2102982. https://doi.org/10.1002/aenm.202102982.
[29] Li CC, Wu Q, Ma J, Pan HG, Liu YX, Lu YY. Regulating zinc metal anodes via novel electrolytes in rechargeable zinc-based batteries. J Mater Chem A. 2022;10:14692. https://doi.org/10.1039/D2TA01672A.
[30] Yang JZ, Yin BS, Sun Y, Pan HG, Sun WQ, Jia BH, Zhang SW, Ma TY. Zinc anode for mild aqueous zinc-ion batteries: challenges, strategies, and perspectives. Nano–micro Lett. 2022; 14(1):1. https://doi.org/10.1007/s40820-021-00782-5.
[31] Li B, Zhang XT, Wang TT, He ZX, Lu BG, Liang SQ, Zhou J. Interfacial engineering strategy for high-performance Zn metal anodes. Nano–micro Lett. 2022;14(1):1. https://doi.org/10.1007/s40820-021-00764-7.
[32] Huang JQ, Chi XW, Du YX, Qiu QL, Liu Y. Ultrastable zinc anodes enabled by anti-dehydration ionic liquid polymer electrolyte for aqueous Zn batteries. ACS Appl Mater Interfaces. 2021;13(3):4008. https://doi.org/10.1021/acsami.0c20241.
[33] Lin CX, Liu YC, Zhang XX, Miao XF, Chen YQ, Chen SJ, Zhang YN. Regulating the plating process of zinc with highly efficient additive for long-life zinc anode. J Power Sources. 2022;549(30):232078. https://doi.org/10.1016/j.jpowsour.2022.232078.
[34] Wang SY, Wang X, Jiang SP. Self-assembly of mixed Pt and Au nanoparticles on PDDA-functionalized graphene as effective electrocatalysts for formic acid oxidation of fuel cells. Phys Chem Chem Phys. 2011;13(15):6883. https://doi.org/10.1039/C0CP02495C.
[35] Paisanpisuttisin A, Poonwattanapong P, Rakthabut P, Ariyasantichai P, Prasittichai C, Siriwatcharapiboon W. Sensitive electrochemical sensor based on nickel/PDDA/reduced graphene oxide modified screen-printed carbon electrode for nitrite detection. RSC Adv. 2022;12(45):29491. https://doi.org/10.1039/D2RA03918D.
[36] Chen T, Jin ZK, Liu YC, Zhang XQ, Wu HQ, Li MX, Feng WW, Zhang Q, Wang C. Stable high-temperature lithium-metal batteries enabled by strong multiple ion-dipole interactions. Angew Chem Int Edit. 2022;61(35):e202207645. https://doi.org/10.1002/anie.202207645.
[37] Muthirulan P, Velmurugan R. Direct electrochemistry and electrocatalysis of reduced glutathione on CNFs-PDDA/PB nanocomposite film modified ITO electrode for biosensors. Colloid Surface B. 2011;83(2):347. https://doi.org/10.1016/j.colsurfb.2010.12.006.
[38] Wang LD, Liu GZ, Zou LJ, Xue DF. Phase evolution from rod-like ZnO to plate-like zinc hydroxysulfate during electrochemical deposition. J Alloy Compd. 2010;493(1–2):471. https://doi.org/10.1016/j.jallcom.2009.12.129.
[39] Gomes A, Silva Pereira MI. Pulsed electrodeposition of Zn in the presence of surfactants. Electrochim Acta. 2006;51(7):1342. https://doi.org/10.1016/j.electacta.2005.06.023.
[40] Sun KEK, Hoang TKA, Doan TNL, Yu Y, Zhu X, Tian Y, Chen P. Suppression of dendrite formation and corrosion on zinc anode of secondary aqueous batteries. ACS Appl Mater Interfaces. 2017; 9(11):9681. https://doi.org/10.1021/acsami.6b16560.
[41] Wei P, Sun XP, He ZM, Cheng FY, Xu J, Li Q, Ren YR, He JH, Han JT, Huang YH. Adenosine triphosphate induced transition-metal phosphide nanostructures encapsulated with N, P-codoped carbon toward electrochemical water splitting. Fuel. 2023;339(1):127303. https://doi.org/10.1016/j.fuel.2022.127303.
[42] Wang T, Sun JM, Hua YB, Krishna BNV, Xi Q, Ai W, Yu JS. Planar and dendrite-free zinc deposition enabled by exposed crystal plane optimization of zinc anode. Energy Storage Mater. 2022;53:273. https://doi.org/10.1016/j.ensm.2022.08.046.
[43] Ding F, Xu W, Graff GL, Zhang J, Sushko ML, Chen XL, Shao YY, Engelhard MH, Nie ZM, Xiao J, Liu XJ, Sushko PV, Liu J, Zhang JG. Dendrite-free lithium deposition via self-healing electrostatic shield mechanism. J Am Chem Soc. 2013;135(11): 4450. https://doi.org/10.1021/ja312241y.
[44] Zhao RR, Wang HF, Du HR, Yang Y, Gao ZH, Qie L, Huang YH. Lanthanum nitrate as aqueous electrolyte additive for favourable zinc metal electrodeposition. Nat Commun. 2022; 13(1):3252. https://doi.org/10.1038/s41467-022-30939-8.
[45] Han YF, Wang JX, Zhang HR, Zhao S, Ma Q, Wang Z. Electrochemical impedance spectroscopy (EIS): an efficiency method to monitor resin curing processes. Sensor Actuat A--Phys. 2016;250(15):7. https://doi.org/10.1016/j.sna.2016.08.028.
[46] Lin CX, Zhang H, Zhang XX, Liu YC, Zhang YN. Kinetics-driven MnO_2 nanoflowers supported by interconnected porous hollow carbon spheres for zinc-ion batteries. ACS Appl Mater Interfaces. 2023;15(11):14388. https://doi.org/10.1021/acsami.3c00067.
[47] Kim S, Lee J, Kang JS, Jo K, Kim S, Sung YE, Yoon J. Lithium recovery from brine using a λ-MnO_2/activated carbon hybrid supercapacitor system. Chemosphere. 2015;125:50. https://doi.org/10.1016/j.chemosphere.2015.01.024.